Plasma-synthesis of various polymorphs of tungsten trioxide nanoparticles using gliding electric discharge in humid air: characterization and photocatalytic properties

Romaric L. SEUTCHA[1], Georges KAMGANG-YOUBI[1,*], Elie ACAYANKA[1], Valeria VERMILE[2], François DEVRED[2], Eric M. GAIGNEAUX[2], Samuel LAMINSI[1]

[1]Inorganic Chemistry Department, Faculty of Sciences, University of Yaounde I, Ngoa-Ekelle 812, Yaoundé, Cameroon

[2]Institute of Condensed Matter and Nanosciences (IMCN), Molecular Chemistry, Materials and Catalysis, Université Catholique de Louvain, Place Louis Pasteur 1, 1348 Louvain-la-Neuve, Belgium

*E-mail of corresponding author: Georges.kamgang@facsciences-uy1.cm

Abstract

Gliding electric arc (glidarc) discharge generates a low temperature plasma at atmospheric pressure. When the discharge occurs in humid air as feeding gas, the chemistry of glidarc plasma consists of in-situ formation HO° and NO° as main primary chemical species. Tungsten trioxide (WO_3) nanoparticles were successfully prepared by exposition of liquid precursor to glidarc plasma. The WO_3 samples were calcined at three different temperatures (300 °C, 500 °C, and 800 °C), resulting to different pure polymorphs: γ-WO_3 (at 300 °C), β-WO_3 (at 500 °C) and α-WO_3 (at 800 °C) according to X-ray diffraction analysis. The identification of WO_3 compounds was also confirmed by ATR FTIR spectroscopy analysis. The increase of the calcination temperature of WO_3 induced the decrease of its specific surface area according to the BET nitrogen physisorption analysis. The UV-vis results showed that the absorption bands of plasma-WO_3 samples were more intense than those of WO_3 samples obtained by precipitation route, a classical method used for comparison. Consequently, this parameter can improve the photocatalytic properties of WO_3 under visible light. The photodegradation (in sunlight conditions) of gentian violet, chosen as pollutant model, confirmed the photocatalytic properties of plasma-WO_3 samples. This novel synthesis method has a great potential to improve the efficiency of advanced tungsten trioxide-based functional material preparation, as well as for the pollution-reducing and energy-saving tungsten extractive metallurgy.

Keywords: glidarc plasma, tungsten trioxide, plasma synthesis, nanoparticles, photocatalyst

(Some figures may appear in colour only in the online journal)

1. Introduction

The need of human being for semiconductors is gradually increasing every day. This is due to their applications in several fields of human activity. Among the main semiconductors used in industries, tungsten trioxide occupies a remarkable place. With the empirical formula WO_3, tungsten trioxide is an oxide whose transition metal is in the $5d^4$ electronic configuration. This semiconductor has been explored extensively in various fields, including gas sensing [1–4]; solar energy conversion; electrochromic displays [5] and catalysis [6–10]. With a small band gap of 2.4–2.8 eV, WO_3 is more effective than titanium dioxide, following the absorption range in visible light region [11]. WO_3 is resistant to degradation through photo-corrosion and could lead to the production of metal ions and a diminution of its catalytic activity. Importantly, oxidation processes on the WO_3 surface are favored by a deep lying valence band (+3.1 eV) [12, 13]. The crystalline structure of chemical sensors and catalysts has a significant impact on their sensitivity, selectivity, and stability [14]. The crystallographic structure of tungsten trioxide is derived from the face-centered cubic structure of rhenium oxide in which the tungsten atoms are located at the vertices of a cube, while the oxygen atoms are in the middle of the edges of the cube [15]. There are several classical techniques to produce tungsten trioxide including precipitation method, ultrasonic synthesis, and thermal oxidation method [16–20].

Recently, we developed a new process for nanocrystalline metal oxides synthesis, involving oxidation or reduction of metal oxide precursors by plasma generated by gliding arc discharge (glidarc), respectively via HO° and NO° plasma-generated species [21–24]. Glidarc plasma is obtained at atmospheric pressure using a simple device and can be classified as non-thermal (low temperature) plasma based on the high temperature gap between electrons and heavy species (ions, radicals, …). Non-thermal plasma is a partially ionized gas with electron temperature much higher than ion temperature. The high-energy electrons and low-energy heavy species can initiate reactions in the plasma volume without excessive heat in contrary of thermal plasmas. Initially developed for the treatment of gases, this technology is also very well suited to the treatment of liquids as detailed in the review paper of Brisset et al [25]. When the gas is humid air, the chemistry of the glidarc plasma involves the production of NO° and HO° radicals as main reactive species [26, 27]. NO° radical is known to be involved in acidifying (HNO_2 and HNO_3) and reducing effects, while HO° radical is involved in the oxidation effects due to its high redox potential $E°_{HO/H2O}$ = 2.85 V/NHE.

Moreover, these primaries species are precursors of other entities such as the reactive oxygen species (ROS) H_2O_2, $°O_2H$; the reactive nitrogen species (RNS) NO_2, HNO_2, NO_2^-, NO_3^-, ONOOH, $ONOO^-$, and the ions O_2^+, O^+, N_2^+, N^+ [25, 28]. Using the redox properties of glidarc plasma species, we recently explored this device to produce metal oxides such as TiO_2, MnO_2, SnO_2 with interesting physicochemical properties [21–24]. In this work, we intend to explore gliding arc plasma-acidic properties to synthesize WO_3 nanoparticles. So, to the best of our knowledge, there is no report for WO_3 synthesis by plasma route.

The aim of this study is to show that we can obtain WO_3 phases (α-WO_3, β-WO_3 and γ-WO_3) with better properties by gliding arc plasma synthesis route. The plasma-obtained material will be compared to the samples obtained by precipitation method in a beaker, which is the method widely used so far. The most important merit of the glidarc plasma process is that it can be considered as a green route, since the reactive species are produced by using a water saturated air which is non-polluting, available, and renewable. Moreover, this novel synthesis technique did not require any reactants adding.

2. Material and methods

2.1. Reagents

To carry out the synthesis of the tungsten trioxide nanoparticles, sodium tungstate dihydrate ($Na_2WO_4•H_2O$) from laboratory grade (Merck, Darmstadt, Germany) was used as precursor. Analytical reagent grade sulfuric acid (H_2SO_4 32 wt.%) was also used in this work for precipitation synthesis route.

2.2. Plasma reactor for synthesis of WO_3 nanoparticles

The non-thermal plasma assembly presented in figure 1 is the experimental device. It has been described previously [23–25]. Briefly, the equipment consists of a generator (a Neon transformer: 9 kV/220 V; 100 mA in open conditions) operating at high voltage, which produces an arc between two diverging electrodes. The plasma power consumption in this condition was then about 100 W. The arc is pushed along the diverging electrodes by humid air flow provided by a compressor and directed along the axis of the two electrodes. The arc glides along the electrodes to their tips where it bursts into a large plasma plume until it is short-circuited and replaced by a new arc. During this process, the temperature of the arc decreases rapidly to a gas temperature of about 800 K and the plasma conductivity is maintained by a high value of the electron temperature of about 10 000 K as determined in previous works using the same reactor [26, 29]. After this

fast transition, the gliding arc continues its evolution, but under non-equilibrium conditions and becomes a quenched plasma close to the ambient temperature and atmospheric pressure. The glidarc plasma density was previously measured through the two main generated species HO° and NO°. In such plasma reactor, the HO° and NO° density measurements were respectively ~10^{18} m^{-3} and ~10^{16} m^{-3} and these values remain constant when moving away from the electrode neck to the target [26]. Furthermore, temperature measurements carried out during the treatment in the target solution exposed to glidarc plasma indicated (8–10) °C higher than room temperature.

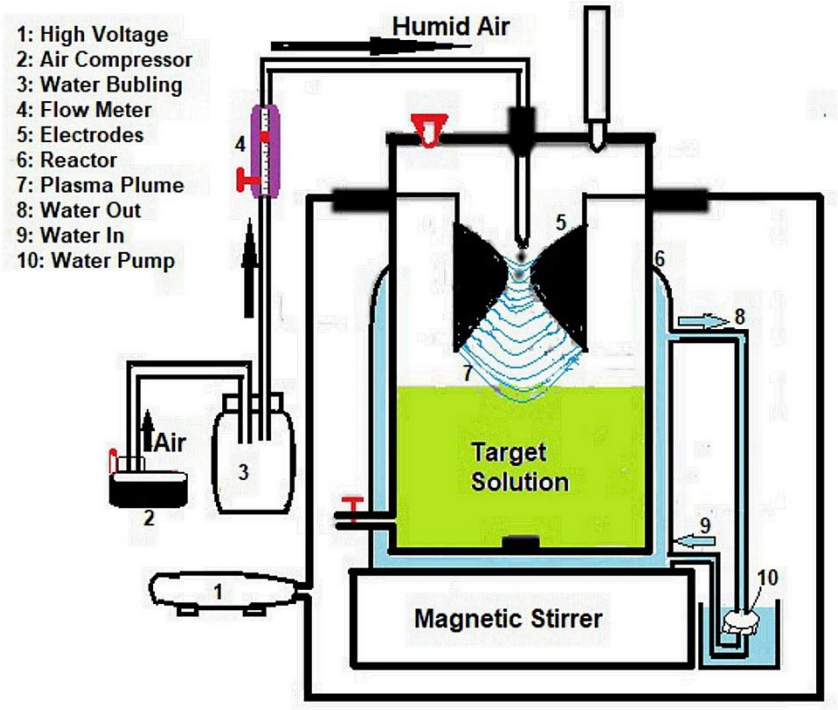

Figure 1. Experimental setup of gliding arc plasma reactor.

2.3. Preparation of WO_3 nanoparticles

2.3.1. In the plasma reactor

For the preparation of WO_3 in the glidarc plasma reactor, 10 g of the precursor ($Na_2WO_4 \cdot H_2O$) was dissolved in 500 ml of distilled water under magnetic stirring. Subsequently, 430 ml of this solution was introduced into the plasma reactor. After connecting the magnetic stirrer, the glidarc plasma experimental

setup was turned on to initiate the synthesis. The flow rate of the plasma gas (humid air) was adjusted to 800 l h^{-1}, the treatment was carried out for 30 min and the exposure solution was recovered after stopping the electric discharge. Filtration allowed the recovery of the paste product formed after leaving the solution to rest for 3 h. Once the paste recovered, it was oven-dried at 100 °C for 8 h. At this stage, the material is hygroscopic, it binds the surrounding air humidity and for this reason, it will be calcined in accordance with the usual methods of synthesis of this oxide [6, 17–19]. Calcination was performed in a muffle furnace (PYRECTRON-PYROLABO, France) by heating the as-synthesized material in an air stream at a heating rate of 10 °C min^{-1}, followed by a 3 h isotherm at desired temperature. Three different calcination temperatures (300 °C, 500 °C and 800 °C for 3 h) were tested.

The samples obtained were named tungsten trioxide "glidarc" (TTG). Arabic numbers have been added to these codes to distinguish calcinated samples at different temperatures. Thus, the codes are TTG1, TTG2 and TTG3 for samples calcinated at 300 °C, 500 °C and 800 °C, respectively.

2.3.2. By precipitation method

Precipitation synthesis route is also carried out in this work to compare with glidarc plasma route. The classical procedure has been described elsewhere [17]. Briefly, 10 g of the same precursor, namely sodium tungstate dihydrate (Na_2WO_4•$2H_2O$), was dissolved in 500 ml of distilled water under magnetic stirrer. Afterwards, a volume of 30 ml of sulfuric acid (32 wt.%) was added while maintaining stirring. After leaving to stand for 3 h, the pale-yellow precipitate of tungsten trioxide hydrate (WO_3•nH_2O) was formed and dried in an oven at 100 °C for 8 h. At this stage, the resulting material was hygroscopic, then it was submitted to the thermal treatments (300 °C, 500 °C and 800 °C during 3 h) to remove structural or chemisorbed water. These calcinations yielded the dry powder of anhydrous composition WO_3. This method leads to obtaining nanometric particles aggregated together [6, 14, 30, 31]. The following equation (1) can be presented to support the synthesis:

$$Na_2WO_4 \bullet 2H_2O \xrightarrow{H_2SO_4\,,\,H_2O} WO_3 \bullet H_2O + 2(Na^+ + HO^-) \xrightarrow{\text{Washing and drying}} WO_{3\,(P)} \quad (1)$$

$WO_{3\,(P)}$ is related to WO_3 obtained by chemical precipitation.

The samples obtained were named tungsten trioxide "precipitation" (TTP) for samples obtained by precipitation method. Arabic numbers have been added to these codes to distinguish calcinated samples at

different temperatures. Thus, the codes are TTP1, TTP2 and TTP3 for samples calcinated at 300 °C, 500 °C and 800 °C respectively.

2.4. Characterization methods

The samples of WO_3 prepared by both methods were characterized through different techniques. X-ray diffraction (XRD) of powders were taken using Bruker D8 X-ray diffractometer, operating in the reflection mode with Cu-Kα radiation (λ = 1.5418 Å, 40 kV, 30 mA) 5°–80° range (2θ) with step of 0.015°, time per step of 0.15 s. ATR Fourier Transform Infrared (ATR-FTIR) was collected in ATR mode using a Bruker Equinox 55 spectrometer equipped with a Platinum ATR cell, in which diamond (refractive index = 2.41) is used as ATR crystal. The spectra were recorded with 100 scans between 4000 and 500 cm^{-1}, resolution of 4 cm^{-1}. Textural analyses were carried out through nitrogen physisorption route on Micromeritics Tristar 3000 apparatus at −196 °C, in the relative pressure range [10^{-6}–0.99]. Samples were previously outgassed at 170 °C under vacuum for minimum 6 h. The BET method was used to calculate the specific surface area, S_{BET}, in the relative pressure range of 0.05–0.30 $P/P°$. The surface morphology of the samples was obtained using a FEI (Field Emission Inspect) scanning electron microscope with a high voltage (HV) of 25 kV. It operates in two vacuum modes (high and low) with secondary and backscattered electron detectors for both vacuum modes. A small quantity of the sample was deposited on a carbon support and filled into the metallizer containing a small among of argon. The micrographs were recorded at the high vacuum mode of the scanning electron microscope. Ultraviolet-visible spectroscopy (UV-vis) spectra were recorded in the wavelength of 200–800 nm, using a Shimadzu UV-3600 Plus spectrophotometer. A Spectralon® Diffuse Reflectance Standard was used to measure the background spectrum. The measured intensity was expressed as the value of the Kubelka–Munk function $F(R)$.

2.5. Photocatalytic applications

Gentian Violet (GV) dye ($C_{25}N_3H_{30}Cl$)) from laboratory grade (Sigma-Aldrich, Missouri, USA) was chosen as pollutant model to study the photocatalytic activity of the synthesized WO_3 nanoparticles. GV is an industrial dye belonging to the triphenylmethane family and is soluble in water [32], its chemical structure is depicted in figure 2.

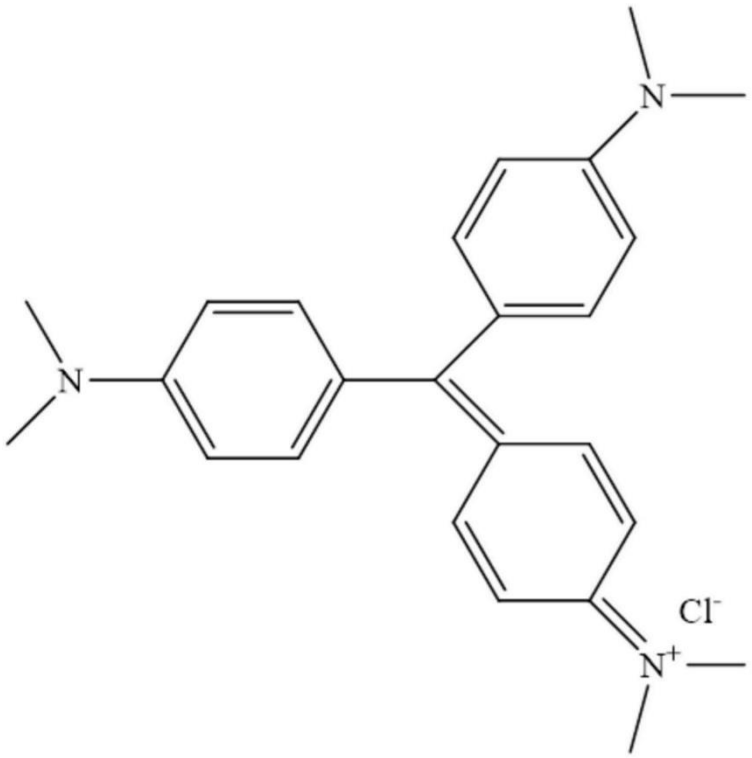

Figure 2. Chemical structure of gentian violet ($C_{25}N_3H_{30}Cl$).

For catalytic studies, a typical experiment consists of 100 ml of 15 mg l^{-1} aqueous dye solution with 75 mg of catalyst taken in a quartz beaker under shaking in a dark for 30 min to reach the adsorption-desorption equilibrium. Then, the suspended solution was irradiated with sunlight for different time intervals. The solar irradiation experiments were conducted from 11:00 am to 3:00 pm at room temperature in Yaounde, Cameroon. During this period, the fluctuation in sunlight intensity is minimal. At the same time, control experiments were realized in similar conditions without catalyst. On the days of experimentation, an average light intensity of 5 kWh m^{-2} day^{-1} was registered using a digital lux meter with 5% accuracy.

At given time intervals, a fraction of the exposed solution was taken and centrifuged at 3600 r min^{-1} for 5 min. The degradation of GV dye was studied by measuring its absorbance at the maximum absorption wavelength (590 nm) with a Lovibond UV-visible spectrophotometer (Spectrodirectanlage 260). The concentration of dye was determined from the calibration curve. The degradation efficiencies (D, %) of the different synthesized WO_3 nanoparticles were determined using the following formula:

$$D\ (\%) = \frac{C_0 - C_t}{C_0} \times 100 \qquad (2)$$

where C_0 and C_t are the initial and at given irradiation time concentration of GV, respectively.

3. Results and discussion

3.1. Synthesis of WO_3 materials

When an aqueous transparent solution of $Na_2WO_4 \bullet 2H_2O$ (white solid) was introduced in the glidarc plasma reactor, its color progressively changed during the 30 min of glidarc plasma exposure (figures 3(a) and (b)). At the end of the step in the plasma reactor, a yellowish paste material was collected (figure 3(c)), then oven-dried at 100 °C for 8 h, resulting in a less pasty material (figure 3(d)). As previously mentioned (section 2.3.1), the obtained material was then calcinated at three different temperatures. The images of the materials after calcination process are presented in the figures 3(e)–(g), respectively for 300 °C, 500 °C and 800 °C. Results indicated that the initial $Na_2WO_4 \bullet 2H_2O$ is converted into solid which will prove to be WO_3 (section 3.2). We can observe an agglomeration of particles to larger ones, which could significantly affect the textural properties of the reference material (WO_3) after removal of structural or chemisorbed water.

Figure 3. Progressive images of WO_3 synthesis by glidarc plasma: (a) aqueous solution of precursor in plasma reactor, (b) aqueous solution during plasma treatment, (c) paste material after plasma synthesis, (d) material

after oven-drying, (e) material calcinated at 300 °C, (f) material calcinated at 500 °C, and (g) material calcinated at 800 °C.

The chemistry of reactive species of humid air plasma describes NO° and HO° radicals as the main entities produced. The HO° radical is the predominant species in cases of oxidation. Suspensions exposed to the glidarc of humid air (parent species: N_2, O_2 and H_2O) have always seen their pH decrease by several units [22, 28, 33]. This acidifying effect is attributed to the NO° radical generated in the plasma plume and induces formation of HNO_2 and HNO_3 (main species responsible of plasma-acidification). It comes from the following reactions (equations (3)–(8)):

$$O_2 + e^- \rightarrow 2\,O^{\circ} + e^- \quad (3)$$

$$N_2 + O \rightarrow NO^{\circ} + N^{\circ} \quad (4)$$

$$N^{\circ} + O^{\circ} \rightarrow NO^{\circ} \quad (5)$$

$$HO^{\circ} + NO^{\circ} \rightarrow HNO_2 \quad (6)$$

$$NO^{\circ} + O^{\circ} \rightarrow NO_2 \quad (7)$$

$$HO^{\circ} + NO_2 \rightarrow HNO_3 \quad (8)$$

In this study, tungsten is the same oxidation state in the precursor $Na_2WO_4{\bullet}2H_2O$ and the synthesized WO_3, thus we should agree that it is the acidifying effect which predominates in this synthesis. In addition, the test for the presence of nitrate ions (NO_3^-) in the supernatant after filtration proved positive. The following equation (9) can then be proposed to explain the plasma synthesis:

$$Na_2WO_4 \bullet 2H_2O + 2\,NO^{\circ} \rightarrow WO_3 \bullet 2H_2O + 2\,(Na^+ + NO_3^-) \xrightarrow{\text{Washing and drying}} WO_{3\,(G)} \quad (9)$$

$WO_{3\,(G)}$ is related to WO_3 obtained by glidarc plasma.

At the end of the calcination step, the different obtained masses were: 4.37 g, 4.35 g, 4.34 g for 300 °C, 500 °C, and 800 °C respectively. The temperature of calcination has practically no influence on the mass of material obtained. According to equation (9), the yields of the synthesis reaction are greater than 60%.

3.2. Characterization of synthesized samples

3.2.1. XRD analysis

Typical XRD patterns of the synthesized tungsten trioxide powder are depicted in figure 4.

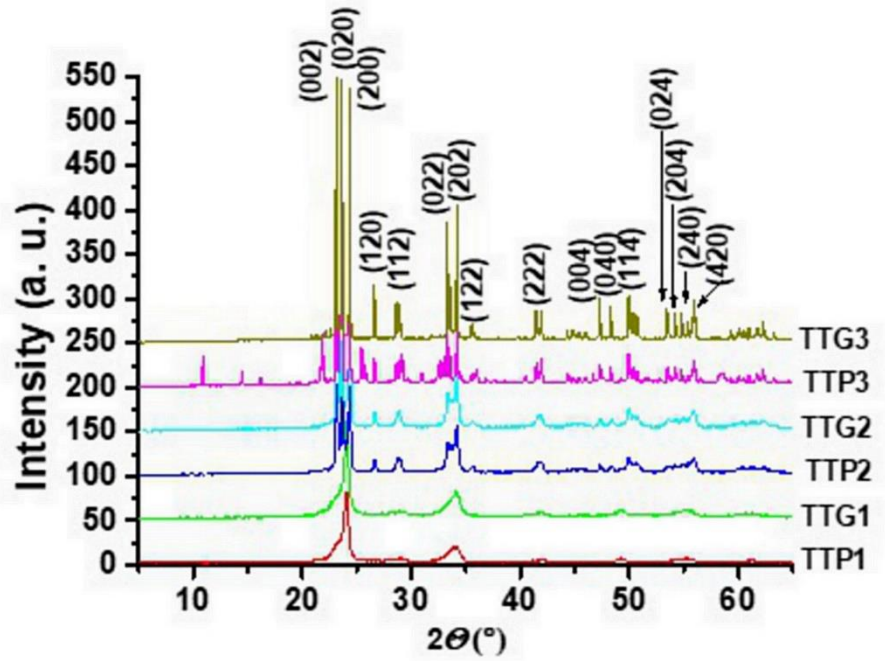

Figure 4. XRD patterns of glidarc plasma synthesized WO_3 (TTG) and precipitated WO_3 (TTP) after calcination at 800 °C (TTG3 and TTP3), 500 °C (TTG2 and TTP2) and 300 °C (TTG1 and TTP1).

XRD profiles of WO_3 samples showed three distinct families of polymorphs: TTP1 with TTG1, TTP2 with TTG2, and TTP3 with TTG3 which correspond respectively to the powders obtained at 300 °C, 500 °C and 800 °C. TTP1 and TTG1 XRD patterns showed two distinct peaks with 2θ at around 23.4°, 34.0° which are characteristics of cubic WO_3 phase (JCPDS 41-0905) [34]. TTP3 and TTG3 XRD patterns showed three main peaks in the range of $23° < 2\theta < 25°$ which indicate together with those at 2θ (33.2°–34.2°) and (50°–56°) that the samples are composed of monoclinic WO_3 (JCPDS 43-1035). TTP3 and TTG3 have very defined peaks, which proves that tungsten trioxide is very crystalline after calcination at 800 °C. But in TTP3 we have extra peaks due to the presence of Na. It means that TTP3 is less ordered or at least less pure compared to TTG3. The monoclinic WO_3 phase characteristically exhibits three large peaks at 2θ values of 23.3°, 23.8° and 24.6° and is the most stable phase at room temperature [35]. Concerning the last polymorph family (TTG2 and TTP2), each sample is a mixture of cubic and monoclinic WO_3 (TTP1 + TTP3 for TTP2,

and TTG1 + TTG3 for TTG2). Indeed, compared to TTG1 (or TTP1), the appearance of new peacks ($25° < 2\theta < 30°$ and $40° < 2\theta < 56°$) is observed in XRD pattern of TTG2 (or TTP2); and these new peaks are well defined in XRD pattern of TTG3 (or TTP3) (JCPDS 83-0950). Overall, the diffraction peaks of metallic tungsten were not detected. All the samples are almost pure. Considering the temperature parameter, XRD results showed that the obtained WO_3 powders (300 °C, 500 °C, 800 °C) correspond respectively to γ-WO_3, β-WO_3 and α-WO_3 phases [36–40]. Regarding the non-calcined sample, in addition to its hygroscopic character mentioned previously, it is well known that its structure is amorphous and only begins to crystallize from 200 °C approximately [41].

The average crystallite sizes (D) of the WO_3 samples (table 1) were evaluated by using Scherrer's equation (10) [20, 42]

$$D = \frac{K \cdot \lambda}{\beta \cdot \cos(\theta)} \tag{10}$$

where K (Scherrer constant: 0.9) is a dimensionless shape factor, λ (0.15418 nm, Cu K_α) is the X-ray wavelength, β is the line broadening at half the maximum intensity (FWHM: full width at half maximum) in radian and θ is the Bragg diffraction angle in radian.

Table 1. Average crystallite sizes (D) of α-WO_3, β-WO_3 and γ-WO_3.

Samples (WO_3)	**TTG1**	**TTP1**	**TTG2**	**TTP2**	**TTG3**	**TTP3**
2theta (2θ degree)	23.9470	24.3346	24.4981	24.2225	23.5047	23.0949
Theta (θ degree)	11.9735	12.1673	12.2490	12.1112	11.7523	11.5474
FWHM (β degree)	0.2598	0.2165	0.2814	0.1732	0.2165	0.1515
WO_3 size D (nm)	**30**	**36**	**27.6**	**45**	**36**	**51**

These results show that the average sizes of WO_3 nanoparticles are ranged between 30 and 36 nm for the glidarc plasma-WO_3 (TTG) samples and between 36 and 51 nm for precipitated-WO_3 samples (TTP). Therefore, the synthesis of WO_3 by glidarc plasma gives smaller nanoparticles sizes compared to the precipitation method. We could observe an increase particle size with the increase of the calcination temperature, which could be ascribed to the removal of structural (chemisorbed) water, inducing an agglomeration of small particles to larger ones and may induce a shrinkage of pores at the surface of material.

3.2.2. ATR Fourier transform infrared characterization

The ATR FTIR spectra of different samples are shown in figure 5.

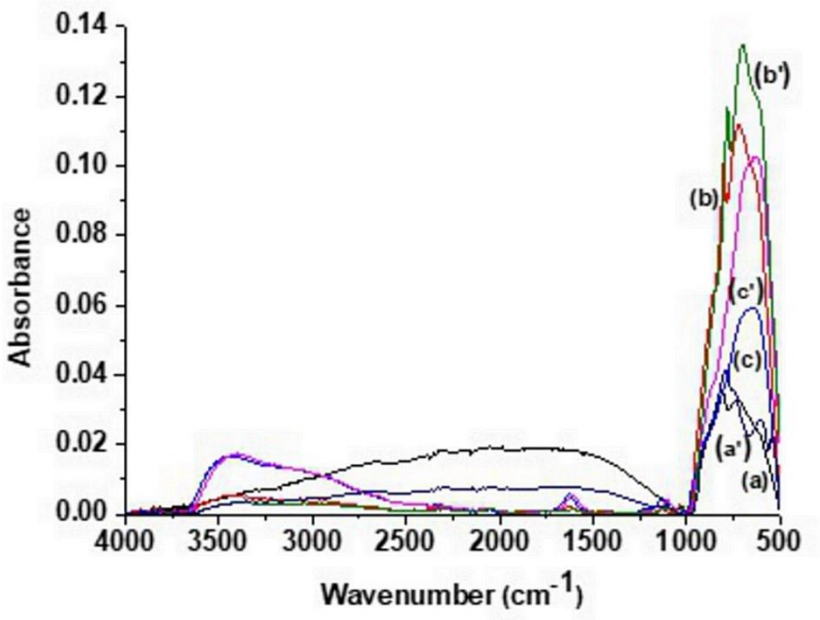

Figure 5. FTIR ATR spectra of glidarc plasma-synthesized WO_3 (TTG) and precipitated WO_3 (TTP) after calcination at 800 °C ((a) TTG3 and (a') TTP3), 500 °C ((b) TTG2 and (b') TTP2) and 300 °C ((c) TTG1 and (c') TTP1).

All the samples show a strong absorption band at 500–1000 cm^{-1}, which is associated with the O–W–O stretching mode. Samples calcined at different temperatures exhibit different profiles in the absorption region between 500 and 1000 cm^{-1}. This can be explained by the different crystalline structures (polymorphs) of powders as previously revealed by XRD analysis. To better interpret these results and get a deep understanding, the association of the spectra as a function of WO_3 structure and synthesis method is shown in figures 6 (for TTP1, TTG1, TTP2 and TTG2) and 7 (for TTP3 and TTG3). These figures highlight the details on the different FTIR ATR spectra.

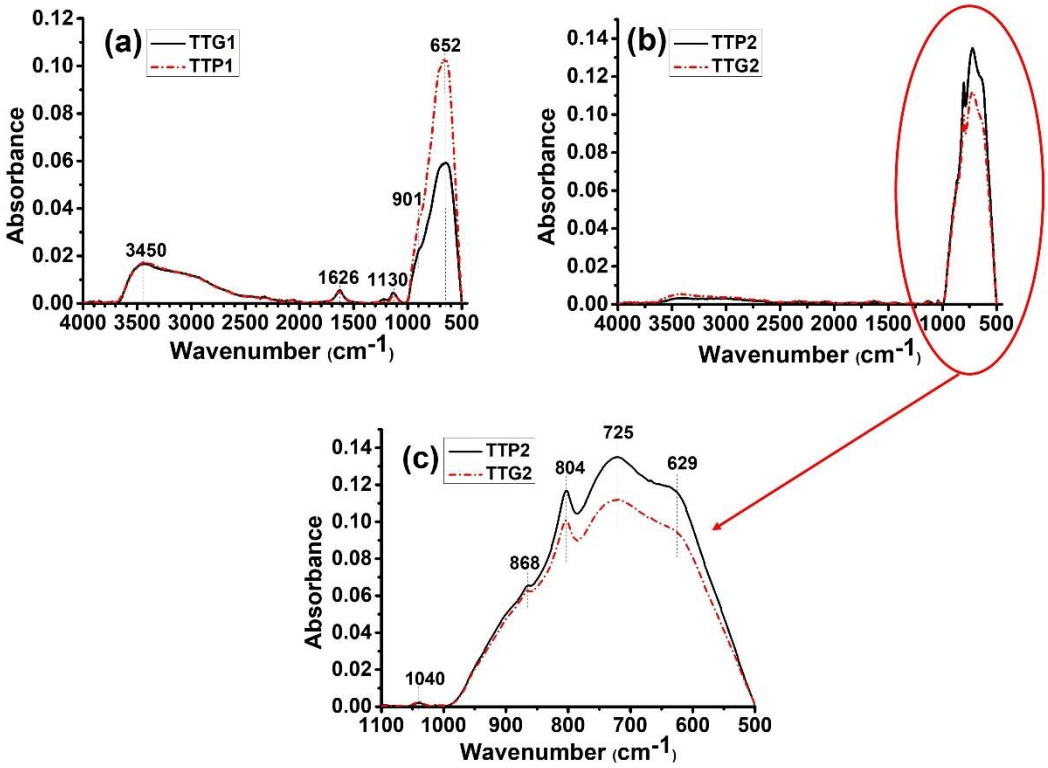

Figure 6. FTIR ATR spectra of glidarc plasma-synthesized WO_3 (TTG) and precipitated WO_3 (TTP) after calcination at (a) 300 °C and (b) 500 °C, (c) a magnification of the area in the range of 500–1000 cm^{-1}.

The spectra of TTP1 and TTG1 (figure 6(a)) show a broad band at 652 cm^{-1} and a shoulder at 901 cm^{-1} which can be ascribed respectively to O–W–O and W=O bonds vibrations. A strong broad band located at 3450 cm^{-1} is assigned to the O–H stretching vibrations of physisorbed water and the band at 1626 cm^{-1} is assigned to the bending H–O–H vibrations of physisorbed water.

The analysis of the TTP2 and TTG2 spectra (figures 6(b) and 6(c)) shows that the samples are practically free of water and could be attributed to calcination at 500 °C releasing physisorbed and chemisorbed waters. Bands between 629 and 868 cm^{-1} are assigned to O–W–O bond stretching. All the samples show a weak band at 1038–1130 cm^{-1} which can be attributed to the stretching of W=O bonds at the surface. These results deeply confirm the presence of WO_3 in these samples.

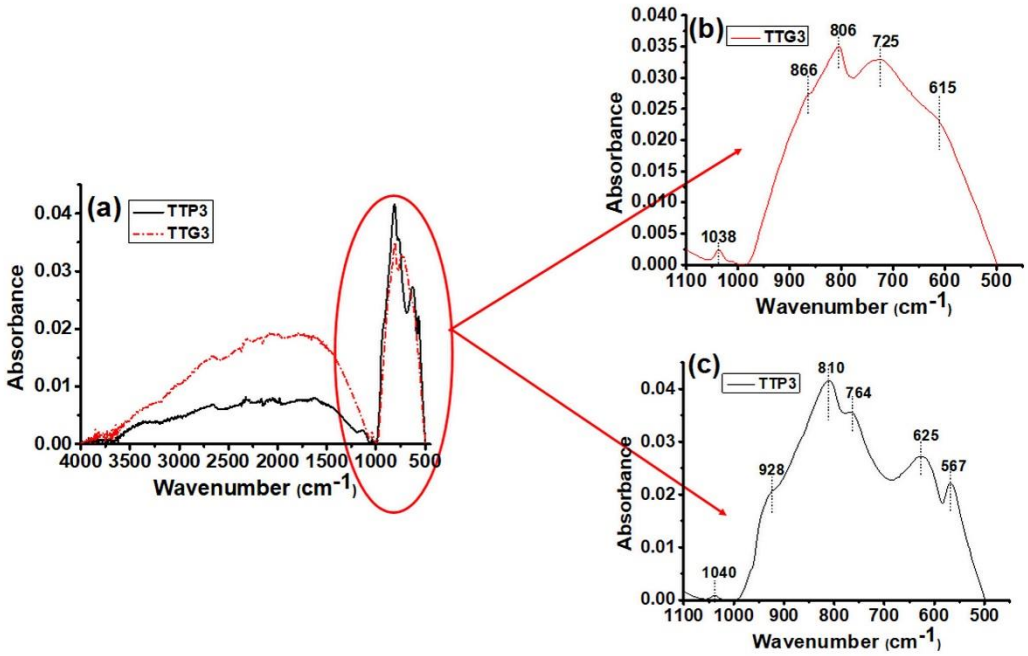

Figure 7. (a) ATR-FTIR spectra of glidarc plasma-synthesized WO_3 (TTG3) and precipitated WO_3 (TTP3) then calcined at 800 °C. The magnification of the area between 500 and 1000 cm^{-1} is also presented for (b) TTG3 and for (c) TTP3.

The stretching and bending vibrations of physisorbed water is observed around 3400 and 1600 cm^{-1}. The previous explanation is also acceptable here. Bands between 615 and 866 cm^{-1} are always due to O–W–O vibrations. The peak at 1038 cm^{-1} is assigned to the stretching of W=O bond. These bands are in different positions in the various samples due to their different calcination temperature, which induces different crystalline structure (polymorphs).

3.2.3. Textural properties of precipitated and glidarc plasma synthesized WO_3

The N_2 adsorption–desorption isotherms of precipitated and glidarc plasma-WO_3 samples are shown in figure 8.

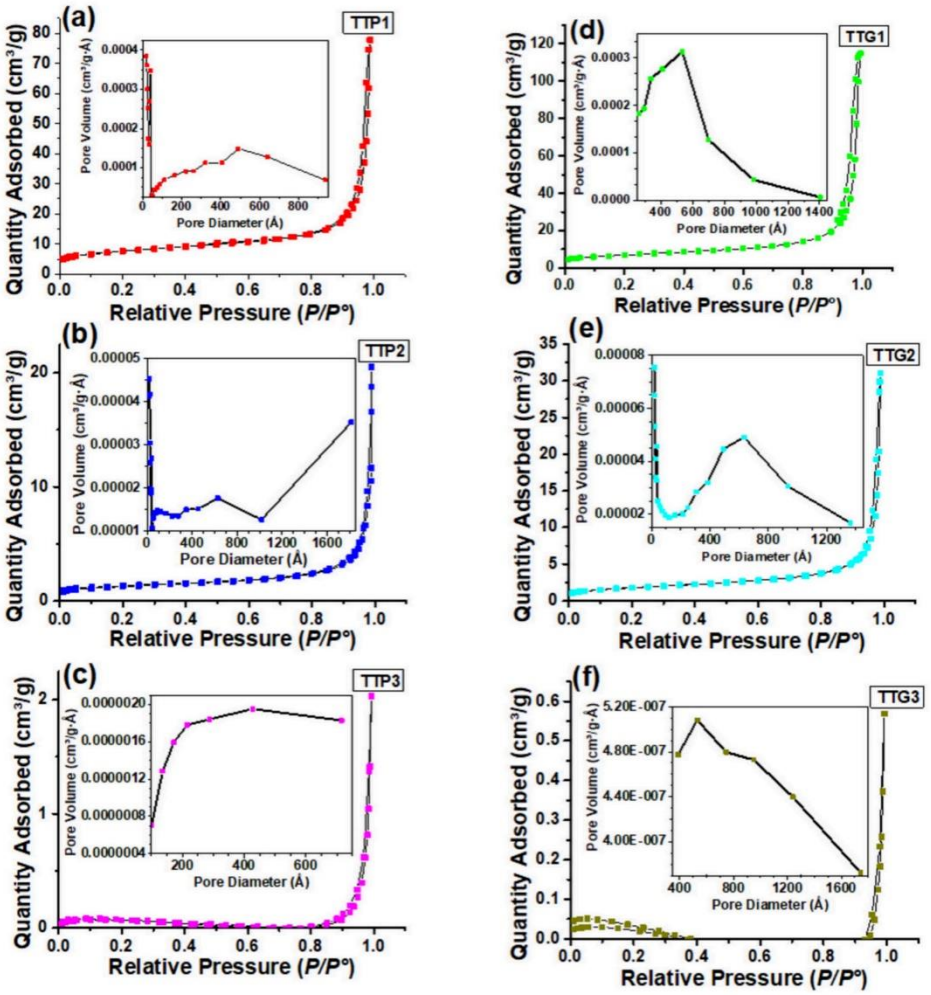

Figure 8. N_2 adsorption–desorption isotherms of glidarc plasma-synthesized WO_3 (TTG1, TTG2, TTG3) and precipitated WO_3 (TTP1, TTP2, TTP3) after calcination at 300 °C ((a) and (d)), 500 °C ((b) and (d)) and 800 °C ((c) and (f)).

All the samples exhibit hysteresis loops in the relative pressure range of 0.8–1.0 typical of IV isotherms, indicating the presence of macropores likely corresponding to voids between non-porous particles [43, 44]. The presence of these macropores is confirmed by the pores size distribution (see insert in the isotherm curves of figure 8). The heterogeneity in the pores size distribution is correlated with the variable particles size. Surface area of WO_3 nanoparticles is important for its use as photocatalyst because sorption phase is one of the controlling factors of the catalytic oxidation reaction. WO_3 nanoparticles with slightly high specific surface area could be obtained at temperatures below 500 °C (e.g. TTP1 and TTG1). For both

TTP and TTG samples, the area of the obtained powders decreased with increasing annealing temperature (table 2).

Table 2. BET surfaces (S_{BET}), pores volumes (V) and pores diameters (D) of different samples.

Sample	S_{BET} ($m^2\ g^{-1}$)	V ($cm^3\ g^{-1}$)	D (Å)	**Sample**	S_{BET} ($m^2\ g^{-1}$)	V ($cm^3\ g^{-1}$)	D (Å)
TTP1	26.0534	0.1136	210.408	**TTG1**	23.9703	0.1523	491.247
TTP2	4.2793	0.0287	329.863	**TTG2**	6.3662	0.0456	313.689
TTP3	0.1454	0.0021	434.560	**TTG3**	0.0284	0.0004	92.229

3.2.4. Microscopy results

Figure 9 shows SEM images of both plasma-synthesized and precipitated samples of WO_3.

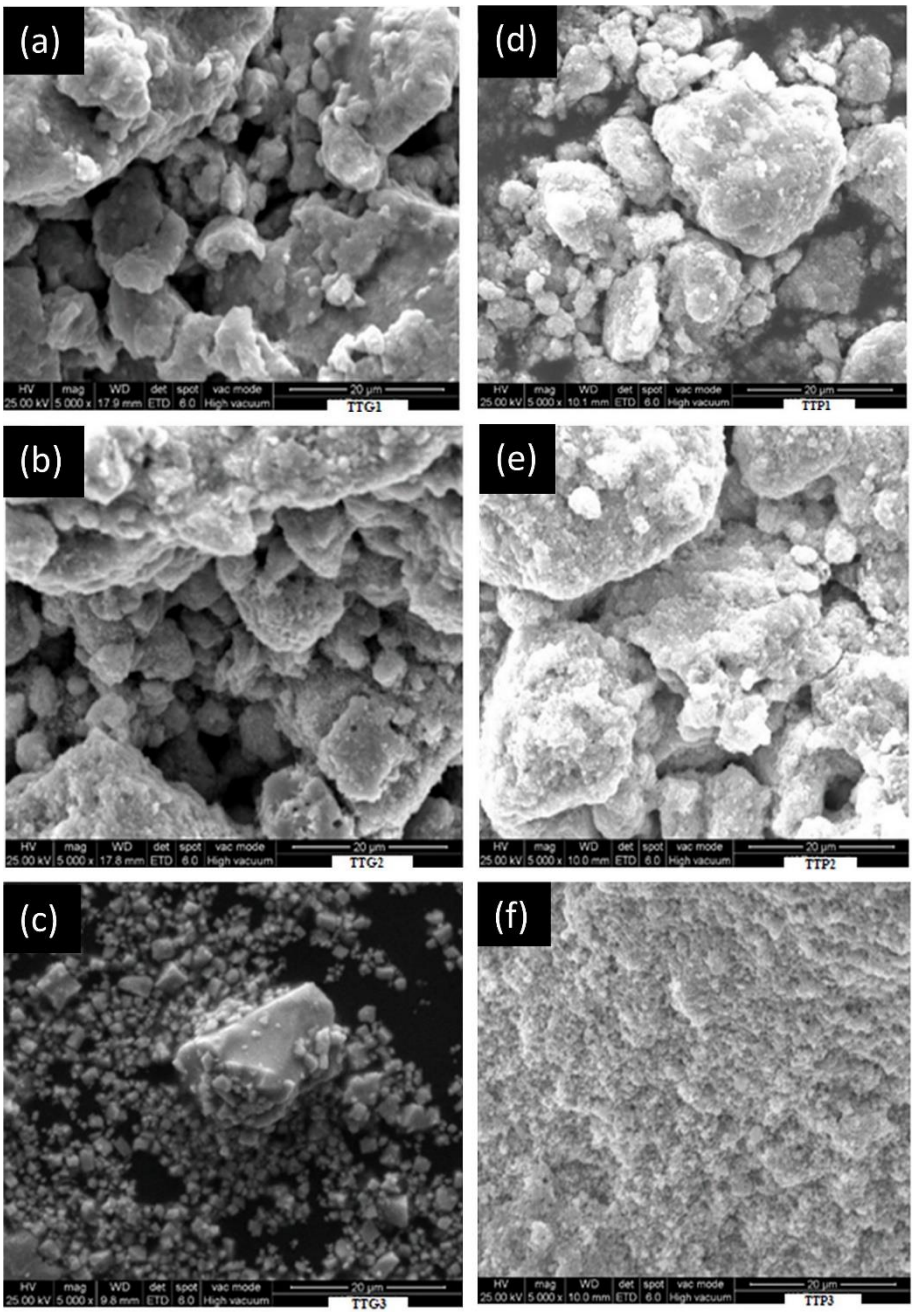

Figure 9. SEM micrographs of glidarc plasma-synthesized WO_3 (left column) and precipitated WO_3 (right column) after calcination at 300 °C (a) TTG1 and (d) TTP1), 500 °C (b) TTG2 and (e) TTP2) and 800 °C (c) TTG3 and (f) TTP3.

The synthesized samples reveal the formation of particles with non-uniform shapes and sizes although the shapes of samples calcinated at 800 °C (TTG3 and TTP3) are likely sand (dusty morphology)

whereas the others (TTG1, TTG2, TTP1 and TTP2) present the shape of gravel (discontinuous spherical morphology). The irregularity in shape and size is well pronounced for the samples calcinated at 300 °C (figures 9(a) and (d)), indicating the presence of mixture of amorphous and crystalline solids. This observation is consistent with the aforementioned XRD results. Figure 9 also shows that the obtained powders are constituted of porous agglomerates, which can be explained by the permanent agitation of the target solution during their synthesis. Moreover, the agglomeration is more pronounced for the samples calcined at 300 °C (figures 9(a) and (d)) and 500 °C (figures 9(b) and (e)) than those calcined at 800 °C (figures 9(c) and (f)) because the temperature rise favors the separation of particles. The surface of WO_3 calcined at 300 °C has a more porous morphology than those calcined at 500 °C and 800 °C. It is known that a porous structure could allow the diffusion of pollutants and subsequently promote an efficient photo-activity.

3.2.5. UV-vis diffuse spectroscopy

Previously, we assessed the impact of calcination temperature on textural properties, which revealed the significant diminution of the specifics surfaces areas of both prepared materials. Therefore, it is relevant to carry out UV-vis spectroscopy analysis. Diffuse reflectance UV–vis spectra of plasma-synthesized WO_3 nanoparticles are depicted in figure 10 and compared to those of precipitated WO_3.

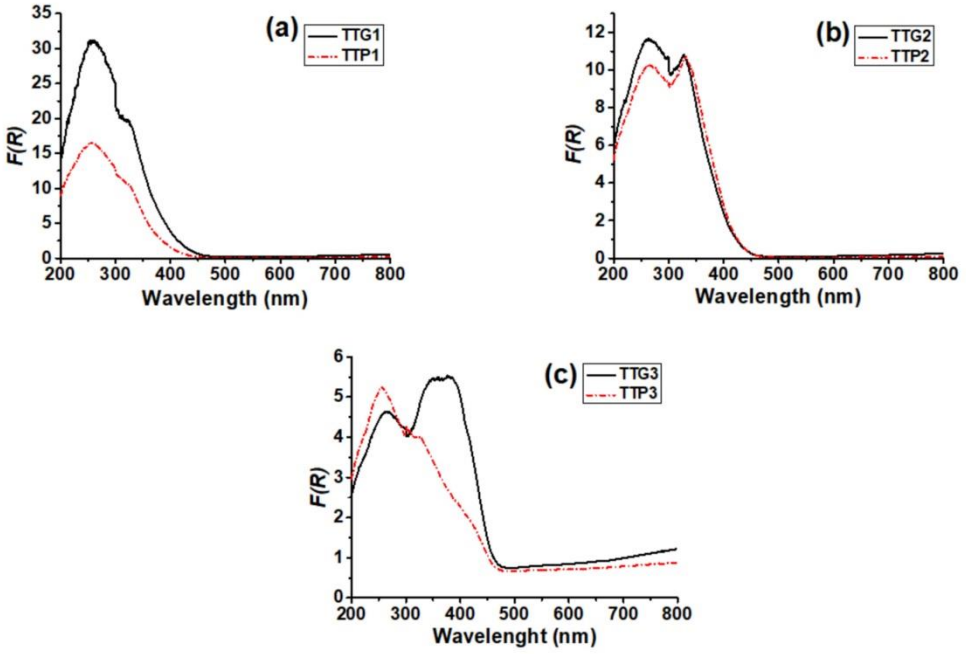

Figure 10. UV–vis diffuse reflectance spectra of glidarc plasma-synthesized WO_3 (TTG) and precipitated WO_3 (TTP) after calcination at (a) 300 °C, (b) 500 °C, and (c) 800 °C.

As shown in figure 10, the band gap energies can be estimated from the intercept of the tangents to the plot's edges. The estimated values for the samples are respectively 2.70 eV, 2.60 eV and 2.57 eV for γ-WO_3 (TTG1), β-WO_3 (TTG2) and α-WO_3 (TTG3) [45]. A significant increase at the absorption wavelengths shorter than 500 nm can be assigned to the intrinsic band-gap absorption of tungsten trioxide due to the electron transitions from the valence band to conduction band O2p → W5d. The increase of UV–absorption edges of plasma-synthesized WO_3 powders to high wavelengths (towards visible region) is useful for improving the photo-absorption and photo-catalytic performance of WO_3 under visible light.

3.3. Photocatalytic applications of synthesized samples

The photocatalytic applications of various glidarc WO_3-polymorphs nanoparticles were studied by evaluating the photodegradation of gentian violet dye under daylight irradiation. The results curves were presented in figure 11.

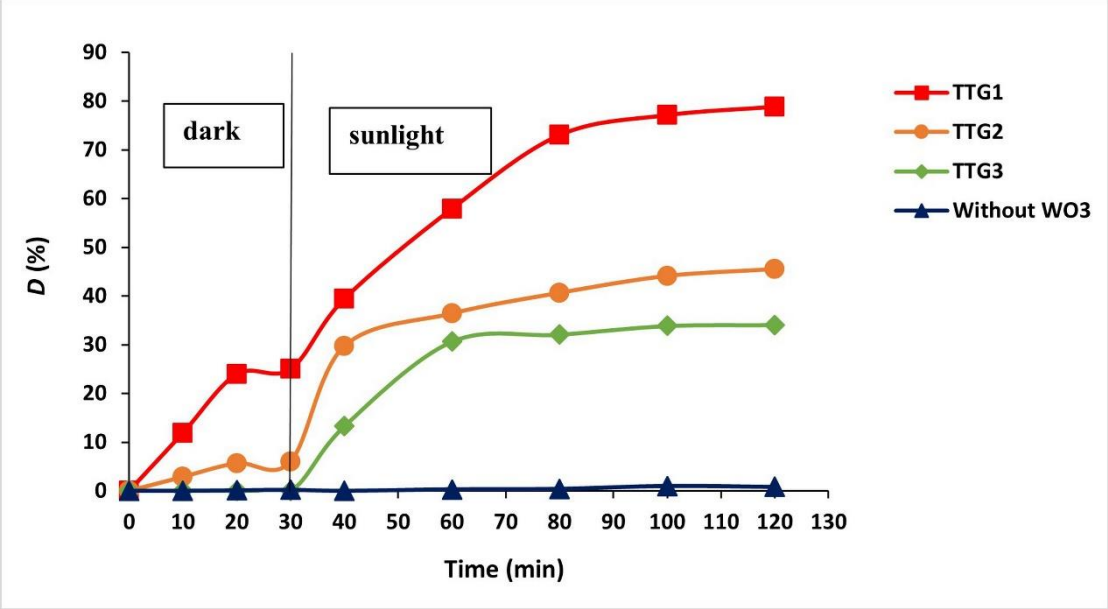

Figure 11. Photodegradation of gentian violet dye without catalyst and over TTG1, TTG2, TTG3.

Photo-destruction of GV alone (without catalyst) does not occur. Under dark conditions, the removal of GV increases gradually and reaches an equilibrium after 20 min of contact regardless of the polymorph used as catalyst. In this condition, adsorption of the pollutant occurs, and the degradation rates at the end of 30 min are: 25%, 6% and 0% for TTG1, TTG2 and TTG3 respectively. The difference in efficiency can be attributed to the difference in specific surface area detailed in paragraph 3.2.3. Indeed, the larger the BET surface area, the higher dye degradation rate is.

In the presence of sunlight, a sudden change in the rate of pollutant degradation is obtained regardless of the polymorph used (figure 11): all the materials synthesized by glidarc plasma are therefore photoactive with respect to the pollutant to be treated. After 90 min of exposure, the degradation rates are 34.05%, 45.54% and 78.86% for TTG3, TTG2 and TTG1 respectively. From these results, the catalytic effect of the materials is clearly highlighted and TTG1 appears to be more efficient than the other samples. A similar trend was previously obtained with another metal (+VI) oxide, MoO_3, synthesized by plasma glow discharge [46] and with TiO_2 synthesized by glidarc plasma [47]. Overall, the photocatalytic activity of the powders obtained decreases with the increase in the annealing temperature. These results confirmed the photocatalytic capacity of tungsten trioxide as demonstrated in previous studies [6, 7, 10]. Furthermore, to confirm the better efficiency of the samples obtained by glidarc plasma synthesis compared to those prepared by precipitation as revealed by the UV-vis properties (figure 10), a comparative study was carried out regarding the same pollutant in the same conditions using TTP1 and TTG1. The degradation curves are presented in the figure 12.

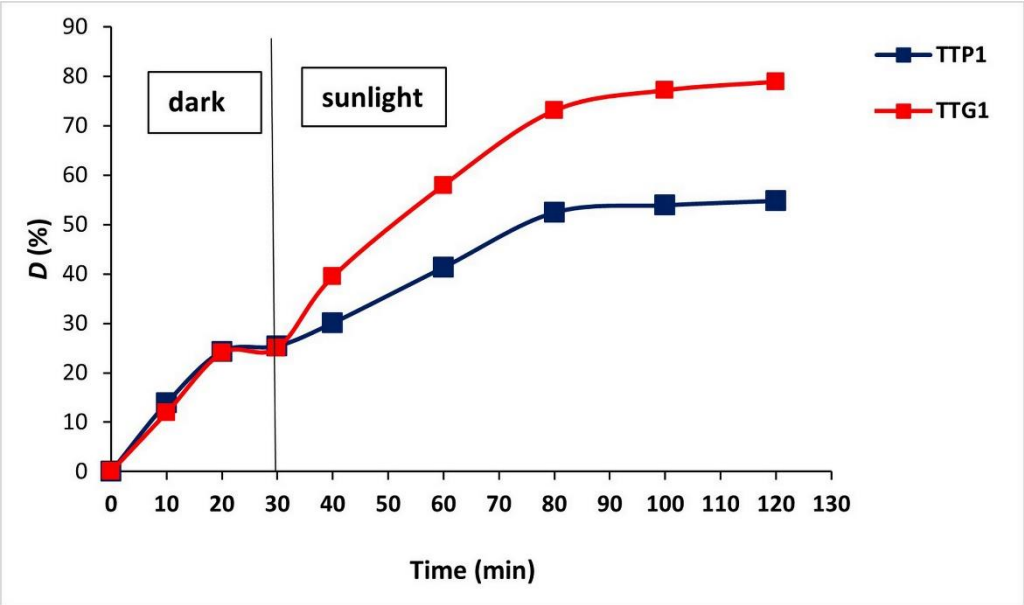

Figure 12. Photodegradation process of gentian violet over TTP1 and TTG1.

Although the levels of degradation under dark are practically similar (which remains consistent with their specific surfaces), the photoactivity of the TTP1 sample (55%) was found to be much lower than that obtained with its counterpart TTG1 (79%). Thus, the increase in UV absorption edges of plasma-synthesized WO_3 powders leads to improved photocatalytic performance under sunlight.

4. Conclusion

Different nanoparticles of WO_3 have been successively prepared by plasma chemical method using gliding arc plasma device. The use of non-thermal quenched plasma at atmospheric pressure favors the formation of active species and free radicals which confer to that process particulars chemical properties. The plume of quenched plasma licks a target solution, and its species react with the $Na_2WO_4 \bullet 2H_2O$ precursor to produce WO_3 nanoparticles through plasma-acidification. The comparison with the one obtained through precipitation showed that the obtained products exhibit the same main crystallographic properties after calcination at different temperatures (300 °C, 500 °C and 800 °C). The XRD revealed that the three obtained phases are crystallized (α-WO_3, β-WO_3 and γ-WO_3). The infrared spectroscopy through bonds identification confirms that tungsten trioxide can be synthesized by gliding arc plasma. However, nitrogen physisorption analysis reveals a significant decrease of the specific surface area as the calcination temperature of WO_3 samples increases. The main difference between the groups of samples is observed on the UV-vis spectra

where the absorption bands of glidarc-WO_3 increase significantly. Indeed, the absorption wavelength of plasma-assisted synthesis of WO_3 increases (diminution of the band gap energy) with the annealing temperature, as compared to the precipitated WO_3 where we recorded the inverse. Their catalytic performance was successfully demonstrated for the degradation of gentian violet dye. Gliding arc plasma can be considered as an easy "green" way to produce WO_3 nanoparticles that can be used for photocatalytic applications under visible light according to this work.

Acknowledgments

The authors owe many thanks to A. Mbouopda-Poupi (UAE University, United Arab Emirates) for performing SEM characterizations.

References

[1] Behera B and Chandra S 2018, *Mater. Sci. Semicond. Process.* **86** 79

[2] Al-Sarraj A *et al* 2022, *Sens. Actuators: A Phys.* **333** 113256

[3] Rout C S, Hegde M and Rao C N R 2008, *Sens. Actuators B Chem.* **128** 488

[4] D'Arienzo M *et al* 2011, *J. Am. Chem. Soc.* **133** 5296

[5] Granqvist C G 2000, *Sol. Energy Mater. Sol. Cells* **60** 201

[6] Razali N A M *et al* 2021, *Mater. Today: Proc.* **42** 22

[7] Gondal M A, Dastageer M A and Khalil A 2009, *Catal. Commun.* **11** 214

[8] Newton K A and Osterloh F E 2016, *Top. Catal.* **59** 750

[9] Rezaee O, Chenari H M and Ghodsi F E 2016, *J. Sol-Gel Sci. Technol.* **80** 109

[10] Ndiffo G B Y *et al* 2021, *Eur. J. Adv. Chem. Res.* **2** 8

[11] Sadakane M *et al* 2011, *Chem. Lett.* **40** 443

[12] Zhao Z G and Miyauchi M 2008, *Angew. Chem. Int.* **47** 7051

[13] Fox M A and Dulay M T 1993, *Chem. Rev.* **93** 341

[14] Uresti D B H *et al* 2014, *Ceram. Int.* **40** 4767

[15] Zou Y S *et al* 2014, *J. Alloys Compds* **583** 465

[16] Ghazal S, Mirzaee M and Darroudi M 2022, *Micro and Nano Lett.* **17** 286

[17] Martínez D S, Solis C G and Martinez L M T 2015, *Mater. Res. Bull.* **61** 165

[18] Verma M, Singh K P and Kumar A 2020, *Solid State Sci.* **99** 105847

[19] Bashirom N and Lee Q L 2020, *Mater. Sci. Forum* **1010** 405

[20] Ding J *et al* 2017, *Appl. Catal. B: Environ.* **203** 335

[21] Acayanka E *et al* 2013, *Plasma Chem. Plasma Process.* **33** 725

[22] Boyom-Tatchemo F W *et al* 2017, *Top. Catal.* **60** 962

[23] Tiya-Djowe A *et al* 2015, *J. Environ. Chem. Eng.* **3** 953

[24] Acayanka E *et al* 2016, *Plasma Chem. Plasma Process.* **36** 799

[25] Brisset J L *et al* 2008, *Ind. Eng. Chem. Res.* **47** 5761

[26] Benstaali B *et al* 2001, *Plasma Chem. Plasma Process.* **22** 553

[27] Delair L, Brisset J L and Cheron B G 2001, *High Temp. Mater. Process.* **20** 381

[28] Kamgang-Youbi G *et al* 2018, *J. Chem. Technol. Biotechnol.* **93** 2544

[29] Fridman A *et al* 1999, *Prog. Energy Combust. Sci.* **25** 211

[30] Guidi V *et al* 2004, *Sens. Actuators B* **100** 277

[31] Amini M *et al* 2014, *New J. Chem.* **38** 1250

[32] Bellir K *et al* 2012, *Energy Procedia* **18** 924

[33] Brisset J L *et al* 2011, *Plasma Sources Sci. Technol.* **20** 034021

[34] Jin G H and Liu S Q 2016, *Dig. J. Nanomater. Biostructures* **11** 763

[35] Bamwenda G R and Arakawa H 2001, *Appl. Catal. A: General* **210** 181

[36] Le Gore L J *et al* 2022, *Thin Solid Films* **406** 79

[37] Hirose T 1980, *J. Phys. Soc. Japan* **49** 562

[38] Salje E 1977, *Acta. Crystallogr. B* **33** 574

[39] Schröder F A 1976, *Acta. Crystallogr. A* **32** 342

[40] Woodward P M, Sleight A W and Vogt T 1995, *J. Phys. Chem. Solids* **56** 1305

[41] Nanba T, Nishiyama Y and Yasui I 1991, *J. Mater. Res*. **6** 6

[42] Deng J *et al* 2022, *Polymer* **43** 2179

[43] Brunauer S *et al* 1940, *J. Am. Chem. Soc.* **62** 1723

[44] Donga P *et al* 2012, *Appl. Surf. Sci.* **258** 7052

[45] Yu J *et al* 2008, *J. Hazard. Mater.* **160** 621

[46] Khlyustova AV *et al* 2019, *Plasma Sci. Technol.* **21** 025505

[47] Mbouopda A P *et al* 2018, *Mater. Chem. Phys.* **206** 224